



This is a repository copy of *Simulating the reactions of substituted pyridinio-N-phosphonates with pyridine as a model for biological phosphoryl transfer*.

White Rose Research Online URL for this paper:

<https://eprints.whiterose.ac.uk/122765/>

Version: Accepted Version

Article:

Pabis, A., Williams, N.H. and Kamerlin, S.C.L. (2017) Simulating the reactions of substituted pyridinio-N-phosphonates with pyridine as a model for biological phosphoryl transfer. *Organic and Biomolecular Chemistry*, 35. pp. 7308-7316. ISSN 1477-0520

<https://doi.org/10.1039/c7ob01734k>

Reuse

Items deposited in White Rose Research Online are protected by copyright, with all rights reserved unless indicated otherwise. They may be downloaded and/or printed for private study, or other acts as permitted by national copyright laws. The publisher or other rights holders may allow further reproduction and re-use of the full text version. This is indicated by the licence information on the White Rose Research Online record for the item.

Takedown

If you consider content in White Rose Research Online to be in breach of UK law, please notify us by emailing eprints@whiterose.ac.uk including the URL of the record and the reason for the withdrawal request.



eprints@whiterose.ac.uk
<https://eprints.whiterose.ac.uk/>

Simulating the Reactions of Substituted Pyridinio-*N*-Phosphonates with Pyridine as a Model for Biological Phosphoryl Transfer

A. Pabis¹, N. H. Williams^{2,*} and S. C. L. Kamerlin^{1,*}

1. Department of Cell and Molecular Biology, Uppsala University, BMC Box 596, S-751 24 Uppsala, Sweden.

2. Department of Chemistry, Sheffield University, Sheffield S3 7HF, United Kingdom

Corresponding author email addresses: kamerlin@icm.uu.se, n.h.williams@sheffield.ac.uk

Abstract

Phosphoryl transfer reactions can proceed through several plausible mechanisms, and the potential for both solvent and substrate-assisted pathways (involving proton transfer to the phosphoryl oxygens) complicates both experimental and computational interpretations. To avoid this problem, we have used electronic structure calculations to probe the mechanisms of the reactions of pyridinio-*N*-phosphonates with pyridine. These compounds avoid the additional complexity introduced by proton transfer between the nucleophile and the leaving group, while also serving as a valuable model for biological P-N cleavage. Through a comparative study of a range of substrates of varying basicity, we demonstrate a unified concerted mechanism for the phosphoryl transfer reactions of these model compounds, proceeding through a dissociative transition state. Finally, a comparison of these transition states with previously characterized transition states for related compounds provides a more complete model for non-enzymatic phosphoryl transfer, which is a critical stepping stone to being able to fully understand phosphoryl transfer in biology.

Keywords: phosphorylated pyridines • phosphoryl transfer • linear free energy relationship • density functional theory • reaction mechanisms

Introduction

Phosphoryl transfer reactions are crucial to biology, being involved in a whole host of processes from cellular signalling to protein synthesis to maintaining the integrity of the genetic material.¹⁻³ Phosphate esters are typically extremely stable, and the half-time for the spontaneous cleavage of these bonds under ambient conditions is typically in the thousands-to-millions of years.⁴ Despite this, the enzymes that catalyse these reactions can achieve phosphoryl transfer on the sub-second timescale, making them among the most proficient characterized.⁴⁻⁸ Therefore, understanding the fundamental mechanisms of how phosphoryl transfer occurs, and how it can be catalysed so proficiently by biological catalysts, is central to understanding a vast range of phenomena involved in the regulation of life,¹⁻³ as well as many of the malfunctions that underlie human disease processes.⁹⁻¹¹ This has been complicated by the fact that the reactions of even simple phosphate monoesters might proceed through different mechanisms (**Scheme 1**), and a large number of (diverse and at times contradictory) mechanistic suggestions have been put forward in the literature on the basis of experimental and computational studies.^{2,3}

As can be seen in **Scheme 1**, phosphoryl transfer reactions plausibly proceed through either solvent- (general base) or substrate-assisted pathways, and the associated transition states can be either tight (associative) or loose (dissociative) in nature, depending on the relative bond orders to the incoming nucleophile and departing leaving group. In addition, although not shown in this scheme, the mechanistic scenarios are further complicated by the possible involvement of phosphorane or metaphosphate intermediates, and that, in principle, the nucleophile can attack from either an inline or a non-inline configuration. Understanding plausible geometries and charge distributions at the transition states for phosphoryl transfer reactions, as well as how the nucleophile is activated, have been key questions in the field.^{2,3} We recently performed detailed quantum chemical studies of the hydrolysis of phosphate monoester dianions^{12, 13} and triphosphates,¹⁴ arguing for a preferred solvent-assisted pathway on the basis of comparison between experimental and calculated activation free energies, linear free energy relationships, and kinetic isotope effects. Specifically, we have demonstrated¹²⁻¹⁴ that this is the only mechanistic model that consistently fits all key experimental observables.

In the present study, we extend our previous computational work¹²⁻¹⁴ to include also an understanding of the reactions of substituted pyridinio-*N*-phosphonates with pyridine, as a model for understanding biological phosphoryl transfer. These compounds have been

experimentally studied in some detail,¹⁵⁻¹⁸ but there have been no corresponding computational studies (although there have been studies of the reactivity of phosphorylated imidazole/histidine¹⁹⁻²¹ as well as studies of linear-free energy relationships and transition states in methoxycarbonyl group transfer between isoquinoline and substituted pyridines²² and proton and methyl transfer between pairs of mimicked 4-substituted pyridines²³). From a computational perspective, a significant advantage of these reactions is that there is no scope for proton transfer between the nucleophile and/or leaving group and the phosphoryl group, which removes the complication of possible substrate-assisted pathways that are available in the hydrolysis of phosphate monoesters and related compounds.¹²⁻¹⁴ This allows us to characterize the nature of the transition state without having to reliably model inter- or intramolecular proton transfer processes at the same time. From an experimental perspective, pyridines have a wide range of basicity for a single structural type,^{24, 25} as well as relatively little steric changes (as long as no ortho substituents are used).²⁶ Finally, from a biological perspective, histidine phosphorylation plays an important role in both prokaryotes and eukaryotes (accounting for 6% of all protein phosphorylation in the latter),²⁷ and, tying in with this, there are an increasing number of crystal structures of enzymes that show histidine phosphorylation (for a review, see ref. ²⁸). As the breakdown of phosphorylated histidine is rapid compared to, for example, phosphoserine,^{7, 29} with the equilibrium strongly favouring the dephosphorylated form,³⁰⁻³³ functionally, histidine phosphorylation is important in a regulatory capacity, for example in signalling systems³⁴ that require organisms to rapidly respond to changing environmental conditions.³⁵⁻³⁷ In addition, histidine phosphorylases form a diverse and evolutionary ancient superfamily of enzymes,³⁸ that are therefore also interesting from an evolutionary perspective. Therefore, it is valuable to have an increased understanding of intrinsic models for biological P-N cleavage.

We provide here a calculated linear free energy relationship (LFER) for the reaction of a range of pyridinio-*N*-phosphonates with pyridine as a nucleophile (**Scheme 2**) that have been experimentally characterized in ref. ¹⁷, and compare the results of these calculations to previous studies of the hydrolysis of phosphate monoesters,^{12, 13} diesters,³⁹ fluorophosphates⁴⁰ and sulfonates.⁴¹ We demonstrate that for all these compounds, the reaction proceeds through a single transition state with inversion of configuration at the phosphorus atom, in good agreement with previous experimental interpretations,¹⁷ and in contrast to recent studies that argue, for example, for metaphosphate intermediates in biological phosphoryl transfer.⁴²⁻⁴⁴ When taken together with previous studies,^{12, 13, 39-41} this provides a more complete

computational model of the intrinsic nature of the transition states involved in biological phosphoryl transfer reactions.

Methodology

Our starting structure for modeling the linear free energy relationship (LFER) for phosphoryl transfer between the pyridinio-*N*-phosphonates and pyridine (**Scheme 2**) was 4-nitropyridine-*N*-phosphate, which acted as the “parent” compound for these simulations. This structure was modeled using a mixed implicit/explicit solvent model, as in our previous studies of phosphate hydrolysis,¹²⁻¹⁴ with eight explicit water molecules carefully positioned to form a symmetrical solvation sphere around the reacting groups. The optimized transition state geometry for this compound was then used as a starting point for optimizing all other transition states of interest, by simply perturbing the leaving group while retaining the same arrangement of water molecules (**Figure S1**). The resulting transition states were characterized by following the intrinsic reaction coordinate (IRC)^{45, 46} in both reactant and product directions, the endpoints of which were optimized to obtain the actual reactant and product complexes (see the **Supporting Information** for coordinates of all stationary points). All stationary points were further characterized by vibrational analysis at the same level of theory as the geometry optimizations. All geometry optimizations were performed using the 6-31+G(d) basis set and the ω B97X-D functional⁴⁷ following our previous work,^{13, 14} and the solvent model density (SMD) continuum model⁴⁸ combined with eight explicit water molecules as described above (see ref. ¹² for detailed discussion and validation of the choice of solvent model). All optimizations were performed using an ultrafine numerical integration grid and tight optimization criteria. Single point energy calculations using a larger 6-311++G(d,p) basis set were performed on all the stationary states, and the final free energies were computed using the zero-point vibrational energies and entropies calculated at the SMD- ω B97X-D/6-31+G(d) level of theory, and the electronic energies obtained with the triple- ζ basis set. Wiberg bond indices⁴⁹ for key stationary points were obtained using natural bond orbital (NBO) analysis⁵⁰ performed on the optimized structures using the same level of theory, and partial charges were calculated using the Merz-Kollman^{51, 52} scheme at the ω B97X-D/6-31G*//SMD- ω B97X-D/6-31+G* level of theory. All calculations in this work were performed using Gaussian 09 (rev. E.01).⁵³

Results and Discussion

In our previous computational studies of the hydrolysis of phosphate monoesters,¹³ triphosphates¹⁴ and sulfonate monoesters,⁴¹ we have compared the performance of a range of DFT functionals, in order to be able to quantify how they discriminate between different mechanistic pathways. We observed that while absolute energies for the hydrolysis of phosphate monoesters and related compounds are highly functional dependent,^{13, 14, 41} the slope of the associated calculated linear free energy relationships was typically very similar irrespective of the functional used.¹³ Based on our previous benchmarking, we have used the ω B97X-D functional in the present study,^{13, 14, 41} as it performed very well in the related hydrolysis of phosphate monoester dianions.¹³

Table 1 shows a comparison between calculated and experimental activation free energies, as well as the experimentally observed rate constants,¹⁷ for the reactions with pyridine of the substituted pyridinio-*N*-phosphonates studied in this work (**Scheme 2**). In all cases, the reaction proceeds through a single, concerted transition state, with the bond distances and bond orders shown in **Table 2**. We note that while the best leaving group for which experimental data exists is isoquinoline (pK_a 5.46), we have extended our calculated LFER to include also pyridine and 4-nitropyridine for comparison. The geometries of key transition states for the compounds with the best and worst leaving groups are shown in **Figure 1** (4-nitropyridine, pK_a 1.61, and 4-aminopyridine, pK_a 9.14, respectively), as well as with pyridine (pK_a 5.23), as this system has an identical nucleophile and leaving group. The Cartesian coordinates of all stationary points are provided as **Supporting Information**. We note that, as shown in **Figure S1**, the geometries of the different transition states overlay very well between the different leaving groups (which is perhaps unsurprising as these were obtained by perturbing a single transition state across the LFER).

The experimental second order rate constants for the reaction of pyridine-*N*-phosphonates with buffers containing added nucleophile (pyridine, *N*, k_{exp}) were obtained from the data presented in **Table 1** of ref.⁵⁴, and the calculated activation free energies were corrected for the entropic cost of bringing the reacting fragments into the reacting cage ($K=0.017\text{ M}^{-1}$), following ref.⁵⁵ and also our previous work^{41, 56}, to yield corresponding calculated second order rate constants. The experimental data yield a Brønsted coefficient, β_{lg} of -0.93, compared to a calculated value of -0.71. For comparison, in the case of the hydrolysis of phosphate monoesters, the experimental β_{lg} is -1.26,^{7, 29} and we obtained a calculated value of -1.51¹³ (**Figure 2**). Therefore, even though our DFT calculations systematically underestimate

the calculated activation free energy (which is a general problem with such calculations that has been discussed in detail elsewhere, *e.g.* in refs.^{41,56-58}) the *relative* trends are in reasonable agreement with experiment, and we obtain a less steep linear relationship for the reactions of pyridinio-*N*-phosphonates compared to phosphate monoester dianions. The scatter in the activation energies for the different substrates might be related to the precise solvation shells for each compounds, and so the extended range of pK_a values has been used to allow a more reliable estimate of the Brønsted plot. We note that, as pointed out by a Reviewer, the calculated Marcus intrinsic barrier of 13.7 kcal mol⁻¹ for the Py/Py identity reaction implies that the thermodynamic range over which the Brønsted slope would be expected to change from 0 (very early transition state) to its maximum value (very late transition state) would be approximately 110 kcal mol⁻¹. This is about 10-fold larger than the energy change for the range of pK_a values for the leaving groups considered in this work, and so leads to an (apparently) linear Brønsted relationship.

Previous experimental studies of these compounds predicted that the electronic nature of the transition state for the reaction shown in **Scheme 3** is (almost) completely independent of the basicity of the nucleophile over a broad range of pK_a values.¹⁷ In addition, the experimentally measured linear/slightly curved Brønsted relationship for the reaction of pyridines with isoquinolinio-*N*-phosphonate indicates that there is a single transition state for a range of nucleophiles.¹⁷ The corresponding observed values of β_{lg} and β_{nuc} are -0.92 and +0.15, respectively, which yields a β_{eq} of $0.15 + 0.92 = 1.07$. This was argued to yield a -0.77 effective charge unit imbalance, that is presumably accommodated by the PO₃ group.¹⁷ When this is combined with the fact that the charge “seen” on the nitrogen is considerably less than 0.5, this suggests a transition state that is in the dissociative corner of a More O’Ferrall-Jencks (MOFJ) plot,^{59, 60} but that is symmetrical in terms of bond cleavage to the incoming nucleophile and departing leaving group if considered in terms of a valence-bond configuration mixing model.⁶¹

Figure 3 shows a comparison of the calculated bond distances and bond orders for the phosphonates studied in this work, and the position of these transition states on the MOFJ plot is shown in **Figure 4**. For comparison, **Figure 4** also shows the position of the transition states for phosphate and sulfonate monoester hydrolyses, with the bond order data taken from the **Supporting Information** of refs.^{13,41}. We have additionally calculated and included bond order data for aryl phosphate diesters and phosphate monoesters from the structures used in our previous studies,^{39, 40} as described in the **Methodology** section. As can be seen from this data, all pyridinio compounds with leaving group pK_a s in the 5.2-6.5 range have very

symmetrical transition states, with the transition states only becoming slightly asymmetric for the compounds at the extremes of the LFER (4-aminopyridine, pK_a 9.14 and 4-nitropyridine, pK_a 1.61). As would be expected, the transition state for pyridine as a leaving group is fully symmetrical. The calculated transition states are tighter than those calculated for the hydrolysis of phosphate monoester dianions,¹³ but still fall clearly in the dissociative (bottom right) corner of the MOFJ shown in **Figure 4**, which is also similar to a recent experimental and computational study of the transition state of phosphoroimidazolid hydrolysis.²⁰ They are also on a spectrum between phosphate monoesters and the tighter transition states observed for the alkaline hydrolysis of phosphate diesters,³⁹ fluorophosphate monoesters⁴⁰ and sulfonate monoesters⁴¹, which are fairly similar in terms of bond orders. Additionally, as in previous cases, the tightness of the transition state is leaving group dependent, with a slight elongation of the P-N_{lg} bond (0.1Å) and contraction of the P-N_{nuc} bond (0.3Å) upon moving from leaving groups with high to low pK_a .

It is worth mentioning that there is a slight asymmetry introduced into the calculations by the position of the explicit water molecules. That is, for example, when we optimize the symmetrical Py/Py transition state in pure implicit solvent, with no additional water molecules (optimized otherwise as described in the **Methodology** section), we obtain P-N_{nuc} = P-N_{lg} = 2.35Å. The introduction of the explicit solvent molecules appears to not just tighten these distances by 0.2Å, but also introduce very slight asymmetry, such that P-N_{nuc} is 0.02Å longer than P-N_{lg}. The calculated reaction free energy (**Table S1**) for this identity reaction is 0.2 kcal mol⁻¹ rather than being isoenergetic. These deviations from symmetry in the case of the identity reaction provide insight into the subtle errors associated with both the energies and geometries presented in this data set. This slight asymmetry could plausibly be removed by ensemble averaging over multiple positions of the different water molecules, although we have not done so here as the errors involved are very small. Tying in with this, even though we refer to the saddle points obtained in this work as “transition states”, these are clearly “a” transition state rather than “the” transition state for each of the systems being studied here, as the real transition state will be an ensemble average over all possible conformations of the water molecules.

The movement of the transition state in figure 4 as the leaving group stability varies does not appear to follow the predictions of a simple analysis. For example, increasing the pK_a of the leaving group might be expected to predominantly lead to increased bonding to the nucleophile in the transition state without changes in the bonding to the leaving group. However, there are evident changes in both. This might be a limitation of the analysis, which

does not take into account potential differential changes in the energy of the intermediate and substrate (*i.e.* the energies along the left hand side of the diagram) as the leaving group is changed. If bonding to the (axial) leaving group in the intermediate is rather weaker than in the substrate, then this corner will also rise in energy and the overall effect on the position of the transition state will have a larger component of Hammond movement. Many of the other substrates illustrated do not include an identity reaction, and involve reaction with hydroxide. That may explain why these substrates appear to have dissociative character, but lie far from the diagonal where the identity reaction would have to fall if the reaction passes through a single transition state during the reaction.

Finally, we have also calculated partial charges using the Merz-Kollman scheme^{51, 52} for each compound studied here, as described in the **Methodology** section, and the corresponding data is shown in **Table 3** and **Figure 4**. We observe in our geometry optimizations that all eight explicit water molecules included in the simulations interact with the non-bridging oxygen atoms of the central phosphate, and not with the nitrogen atoms of the incoming nucleophile and departing leaving group (see **Figure 2**). As can be seen from the calculated partial charges, both leaving group and nucleophile pyridyl groups carry a positive partial charge of, on average, 0.337 ± 0.044 on the nucleophilic pyridyl group (Py_{nuc}), 0.392 ± 0.027 on the leaving group pyridyl (Py_{lg}), and -1.769 ± 0.031 on the central PO_3 group (we note that our charges are more polarized than the experimental estimate). In addition, there is a shift to a more positive partial charge on Py_{nuc} , a less positive partial charge on Py_{lg} , and a more negative partial charge on PO_3 respectively when moving across the series, in line with the observed changes in bond order.

Overview and Conclusions

Past decades have seen significant debate about the nature of the transition states involved in phosphoryl transfer reactions, with contradictory propositions in the literature based on both experimental and computational data.^{2, 3} We were recently able to reconcile long-standing controversies between experimental and computational interpretations of the mechanisms of phosphate monoester hydrolysis through the use of high-level quantum chemical calculations coupled with a mixed solvent model that allowed for microsolvation of the highly charged phosphate, allowing us to optimize a dissociative, solvent-assisted transition state.¹² This provided, for the first time, a computational model for phosphate monoester hydrolysis consistent with all key experimental observables, including the

experimental linear free energy relationship,¹³ and also measured kinetic isotope effects.¹² We extend our previous work here to modelling the reaction of substituted pyridinio-*N*-phosphonates with pyridine as nucleophile, which eliminates the additional computational complexity when studying phosphate monoesters due to protonation of the nucleophile and leaving group. We demonstrate that these reactions proceed through a single, concerted transition state that is dissociative in nature, with no intermediates, and which is slightly tighter than the corresponding transition state for the hydrolysis of phosphate monoester dianions.^{12, 13} We note that phosphorylated histidine is a major participant in signal transduction pathways,³⁴ and, although less well studied, phosphorylation of both arginine and lysine residues is also biologically important.⁶² This work therefore also provides an important foundation for subsequent computational studies of the mechanisms of biological P-N cleavage.

Acknowledgments

This work was funded by a Wenner-Gren Foundations Postdoctoral Fellowship to Anna Pabis. All computational work was performed on the Kebnekaise cluster at HPC2N in Umeå, and the Rackham cluster at UPPMAX in Uppsala, through a generous allocation of computational time from the Swedish National Infrastructure for Computing (SNIC Grant 2016-34-27).

References

1. F. H. Westheimer, *Science*, 1987, **235**, 1173-1178.
2. J. K. Lassila, J. G. Zalatan and D. Herschlag, *Annu. Rev. Biochem.*, 2011, **80**, 669-702.
3. S. C. L. Kamerlin, P. K. Sharma, R. B. Prasad and A. Warshel, *Q. Rev. Biophys.*, 2013, **46**, 1-132.
4. R. Wolfenden, *Chem. Rev.*, 2006, **106**, 3379-3396.
5. A. Radzicka and R. Wolfenden, *Science*, 1995, **267**, 90-93.
6. R. Wolfenden, C. Ridgway and G. Young, *J. Am. Chem. Soc.*, 1998, **120**, 833-834.
7. C. Lad, N. H. Williams and R. Wolfenden, *Proc. Natl. Acad. Sci. U. S. A.*, 2003, **100**, 5607-5610.
8. G. K. Schroeder, C. Lad, P. Wyman, N. H. Williams and R. Wolfenden, *Proc. Natl. Acad. Sci. U. S. A.*, 2006, **103**, 4052-4055.
9. J. den Hertog, *EMBO Rep.*, 2003, **4**, 1027-1032.

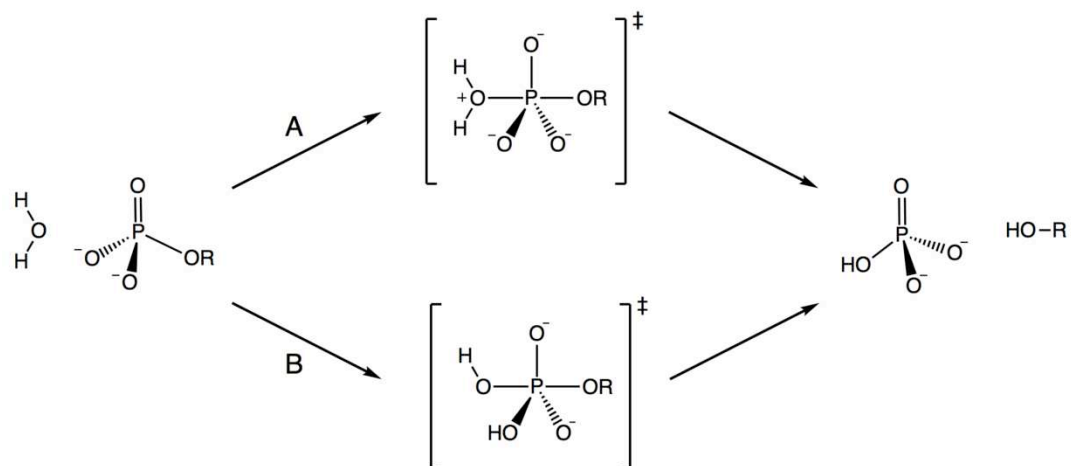
10. N. K. Tonks, *Protein tyrosine phosphatases: from genes, to function, to disease.*, 2006, **7**, 833-846.
11. G. A. Hobbs, C. J. Der and K. L. Rossman, *J. Cell Sci.*, 2016, **129**, 1287-1292.
12. F. Duarte, J. Åqvist, N. H. Williams and S. C. L. Kamerlin, *J. Am. Chem. Soc.*, 2015, **137**, 1081-1093.
13. F. Duarte, A. Barrozo, J. Åqvist, N. H. Williams and S. C. L. Kamerlin, *J. Am. Chem. Soc.*, 2016, **138**, 10664-10673.
14. A. Barrozo, D. Blaha-Nelson, N. H. Williams and S. C. L. Kamerlin, *Pure Appl. Chem.*, 2017, **In Press**, DOI: <https://doi.org/10.1515/pac-2016-1125>.
15. M. T. Skoog and W. P. Jencks, *J. Am. Chem. Soc.*, 1983, **105**, 3356-3357.
16. M. T. Skoog and W. P. Jencks, *J. Am. Chem. Soc.*, 1984, **106**, 7597-7606.
17. N. Bourne and A. Williams, *J. Am. Chem. Soc.*, 1984, **106**, 7591-7596.
18. D. Herschlag and W. P. Jencks, *J. Am. Chem. Soc.*, 1989, **111**, 7587-7596.
19. S. Sharma, A. Rauk and A. H. Juffer, *J. Am. Chem. Soc.*, 2008, **130**, 9708-9716.
20. L. Li, V. C. Lelyveld, N. Prywes and J. W. Szostak, *J. Am. Chem. Soc.*, 2016, **138**, 3986-3989.
21. E. S. Orth, T. A. S. Brandao, B. S. Souza, J. R. Pliego, B. G. Vaz, M. N. Eberlin, A. J. Kirby and F. Nome, *J. Am. Chem. Soc.*, 2010, **132**, 8513-8523.
22. I. H. Williams and P. A. Austin, *Can. J. Chem.*, 1999, **77**, 830-841.
23. R. B. Hammond and I. H. Williams, *J. Chem. Soc. Perkin Trans. II*, 1989, 59-66.
24. E. A. Castro and R. B. Moodie, *J. Chem. Soc., Chem. Commun.*, 1973, 828-829.
25. P. M. Bond, E. A. Castro and R. B. Moodie, *J. Chem. Soc., Perkin Trans.*, 1976, 68-72.
26. G. W. Jameson and J. M. Lawlor, *J. Chem. Soc.*, **1970**, 53-57.
27. H. R. Matthews, *Pharm. Ther.*, 1995, **67**, 323-350.
28. J. Puttick, E. N. Baker and L. T. J. Delbaere, *Biochim. Biophys. Acta - Proteins Proteom.*, 2008, **1784**, 100-105.
29. N. H. Williams, *Biochim. Biophys. Acta*, 2004, **1697**, 279-287.
30. B. S. Cooperman and G. J. Lloyd, *J. Am. Chem. Soc.*, 1971, **93**, 4883-4889.
31. J. B. Stock, A. M. Stock and J. M. Mottonen, *Nature*, 1990, **344**, 395-400.
32. P. V. Attwood, M. J. Piggott, X. L. Zu and P. G. Besant, *Amino Acids*, 2007, **32**, 145-156.
33. E. S. Orth, E. H. Wanderlind, M. Medeiros, P. S. M. Oliveira, B. G. Vaz, M. N. Eberlin, A. J. Kirby and F. Nome, *J. Org. Chem.*, 2011, **76**, 8003-8008.

34. S. Klumpp and J. Krieglstein, *Eur. J. Biochem.*, 2002, **269**, 1067-1071.
35. A. M. Stock, V. L. Robinson and P. N. Goudreau, *Annu. Rev. Biochem.*, 2000, **69**, 183-215.
36. T. Mascher, J. D. Helmann and G. Udden, *Microbiol. Mol. Biol. Rev.*, 2006, **70**, 910-938.
37. K. Jung, L. Fried, S. Behr and R. Heermann, *Curr. Opin. Microbiol.*, 2012, **15**, 118-124.
38. D. J. Rigden, *Biochem. J.*, 2008, **409**, 333-348.
39. E. Rosta, S. C. L. Kamerlin and A. Warshel, *Biochemistry-Us*, 2008, **47**, 3725-3735.
40. A. Alkherraz, S. C. L. Kamerlin, G. Feng, Q. I. Sheikh, A. Warshel and N. H. Williams, *Faraday Discuss.*, 2010, **145**, 281-299.
41. F. Duarte, T. Geng, G. Marloie, A. O. Al Hussain, N. H. Williams and S. C. L. Kamerlin, *J. Org. Chem.*, 2014, **79**, 2816-2828.
42. F. A. Kiani and S. Fischer, *Phys. Chem. Chem. Phys.*, 2016, **18**, 20219-20233.
43. F. A. Kiani and S. Fischer, *Curr. Opin. Struct. Biol.*, 2015, **31**, 115-123.
44. V. Prado, E. Lence, J. A. Vallejo, A. Beceiro, P. Thompson, A. R. Hawkins and C. Bonzález-Bello, *Chem. Eur. J.*, 2016, **22**, 2758-2768.
45. H. P. Hratchian and H. B. Schlegel, *J Chem Phys*, 2004, **120**, 9918-9924.
46. H. P. Hratchian and H. B. Schlegel, *J. Chem. Theory Comput.*, 2005, **1**, 61-69.
47. J. D. Chai and M. Head-Gordon, *Phys. Chem. Chem. Phys.*, 2008, **10**, 6615-6620.
48. A. V. Marenich, C. J. Cramer and D. G. Truhlar, *J. Phys. Chem. B*, 2009, **113**, 6378-6396.
49. K. B. Wiberg, *Tetrahedron*, 1968, **24**, 1083-1096.
50. J. P. Foster and F. Weinhold, *J. Am. Chem. Soc.*, 1980, **102**, 7211-7218.
51. U. C. Singh and P. A. Kollman, *J. Comput. Chem.*, 1984, **5**, 129-145.
52. B. H. Besler, K. M. Merz Jr. and P. A. Kollman, *J. Comput. Chem.*, 1990, **11**, 431-439.
53. M. J. Frisch, G. W. Trucks, H. B. Schlegel, G. E. Scuseria, M. A. Robb, J. R. Cheeseman, G. Scalmani, V. Barone, B. Mennucci, G. A. Petersson, H. Nakatsuji, M. Caricato, X. Li, H. P. Hratchian, A. F. Izmaylov, J. Bloino, G. Zheng, J. L. Sonnenberg, M. Hada, M. Ehara, K. Toyota, R. Fukuda, J. Hasegawa, M. Ishida, T. Nakajima, Y. Honda, O. Kitao, T. Nakai, T. Vreven, J. A. Montgomery Jr., J. E. Peralta, F. Ogliaro, M. Bearpark, J. J. Heyd, E. Brothers, K. N. Kudin, V. N. Staroverov, R. Kobayashi, J. Normand, K. Raghavachari, A. Rendell, J. C. Burant, S.

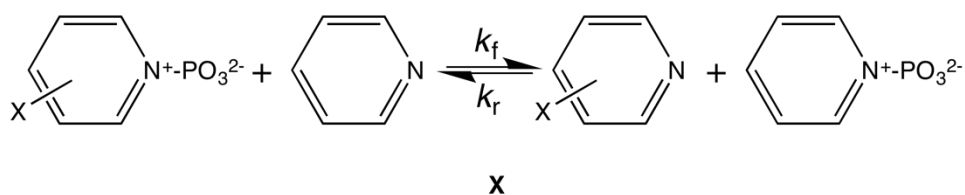
- S. Iyengar, J. Tomasi, M. Cossi, N. Rega, J. M. Millam, M. Klene, J. E. Knox, J. B. Cross, V. Bakken, C. Adamo, J. Jaramillo, R. Gomperts, R. E. Stratmann, O. Yazyev, A. J. Austring, R. Cammi, C. Pomelli, J. W. Ochterski, R. L. Martin, K. Morokuma, V. G. Zakrzewski, G. A. Voth, P. Salvador, J. J. Dannenberg, S. Dapprich, A. D. Daniels, Ö. Farkas, J. B. Foresman, J. V. Ortiz, J. Cioslowski and D. J. Fox, *Gaussian 09, Revision E.01*, Gaussian Inc., Wallingford CT.
54. N. Bourne and A. Williams, *J. Org. Chem.*, 1984, **49**, 1200.
55. J. Hine, *J. Am. Chem. Soc.*, 1971, **93**, 3701-3708.
56. F. Duarte, S. Gronert and S. C. L. Kamerlin, *J. Org. Chem.*, 2014, **79**, 1280-1288.
57. J. Ho and M. Z. Ertem, *J. Phys. Chem. B*, 2016, **120**, 1319-1329.
58. M. Li, X. Yang and Y. Xue, *Theor. Chem. Acc.*, 2017, **136**, 69.
59. R. A. O’Ferrall, *J. Chem. Soc. B*, 1970, DOI: Doi 10.1039/J29700000274, 274–277.
60. W. P. Jencks, *Chem. Rev.*, 1985, **85**, 511-527.
61. A. Pross and S. S. Shaik, *Acc. Chem. Res.*, 1983, **16**, 363-370.
62. P. V. Altwood, *Biochim. Biophys. Acta*, 2013, **1834**, 470-478.
63. J. M. Essery and K. Schofield, *J. Chem. Soc.*, 1963, 2225-2227.
64. A. Albert, R. Goldacre and J. Phillips, *J. Chem. Soc.*, 1948, 2240-2249.

Figures and Tables

Scheme 1: Comparison of (A) solvent- and (B) substrate-assisted pathways for phosphate monoester hydrolysis.



Scheme 2: Pyridinio-N-phosphonates studied in this work.



- X**
- 1 pyridine
 - 2 4-nitropyridine
 - 3 3-methylpyridine
 - 4 3-aminopyridine
 - 5 3,4-dimethylpyridine
 - 6 4-aminopyridine
 - 7 isoquinoline

Figure 1: Calculated transition states for the reactions of pyridine with different pyridinio-*N*-phosphonates, where the leaving group is either (**left**) 4-aminopyridine (pK_a 9.14), (**middle**) pyridine (pK_a 5.23) or (**right**) 4-nitropyridine (pK_a 1.61). Coordinates for all stationary points can be found as supporting information.

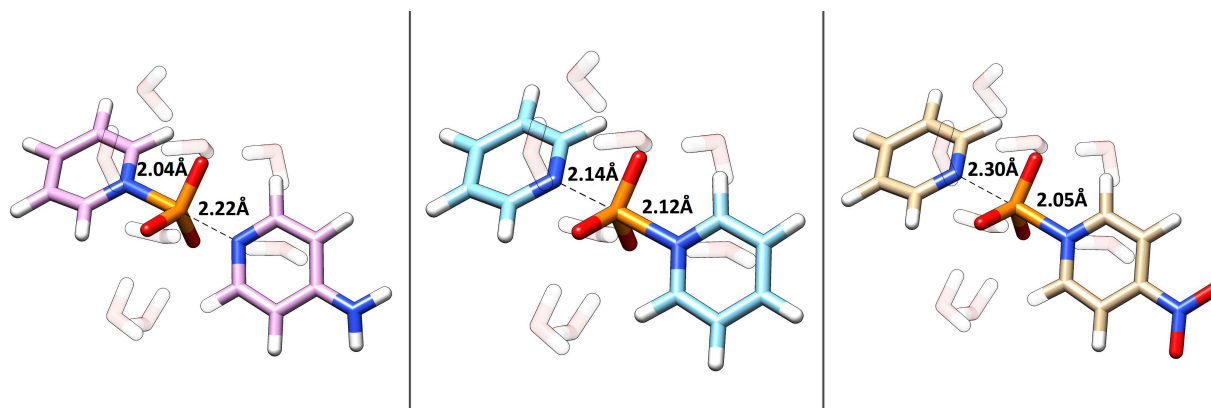


Figure 2: Calculated (black) and experimental (red) LFER for the reactions of (A) pyridine with pyridinio-N-phosphonates^a and (B) solvent-assisted monoester hydrolysis from our previous study^{b,13}. Calculated rate constants were obtained from the corresponding activation free energies using transition state theory. Energy calculations were performed at 298.15 K using SMD- ω B97X-D/6-31+G(d) level of theory. The experimental values were obtained from ref. ¹⁷, and the pseudo-first order rate constants were obtained by correcting for the entropic cost of bringing the reacting fragments into the reacting cage ($K=0.017\text{ M}^{-1}$), following ref. ⁵⁵. ^b Reported rate constants were obtained using SMD- ω B97X-D/6-311++G(d,p)//SMD- ω B97X-D/6-31+G(d) level of theory. For further details of the methodology and the experimental data, see ref. ¹³.

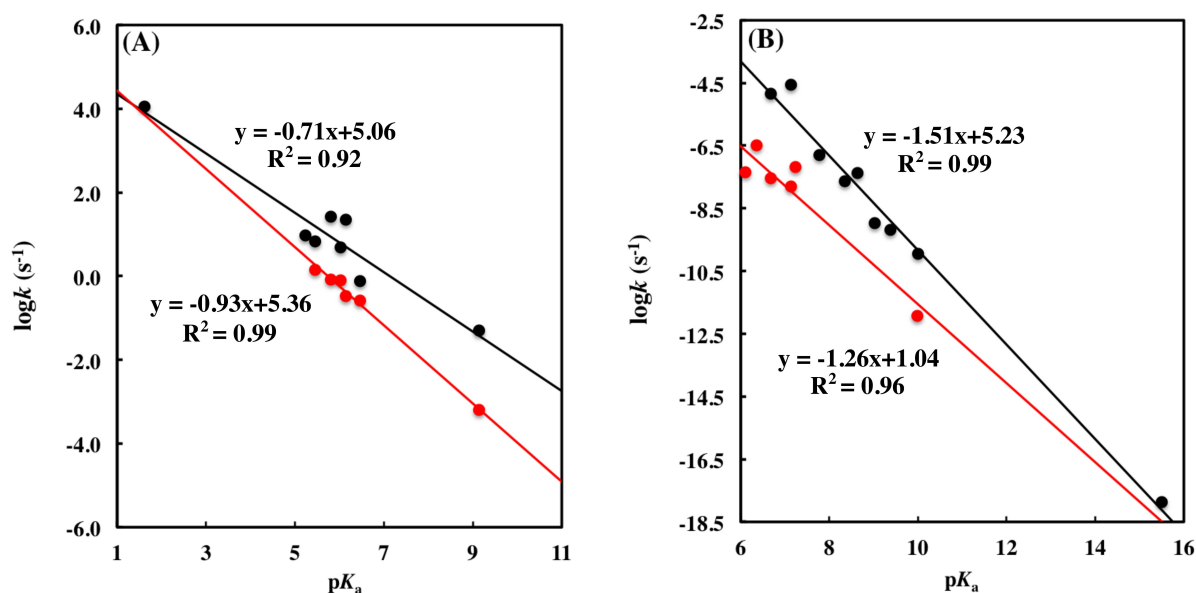


Figure 3: Calculated P-N distances (**A**) of the incoming nucleophile ($P-N_{\text{nuc}}$, black circles) departing leaving group ($P-N_{\text{lg}}$, blue circles) and corresponding Wiberg bond indices⁴⁹ (**B**) for the transition states for the reaction of pyridine with pyridinio-N-phosphonates shown in **Scheme 2** optimized at SMD- ω B97X-D/6-31+G(d) level of theory. Wiberg bond indices were calculated using natural orbital (NBO) analysis⁵⁰ at the same level of theory, as described in the **Methodology** section.

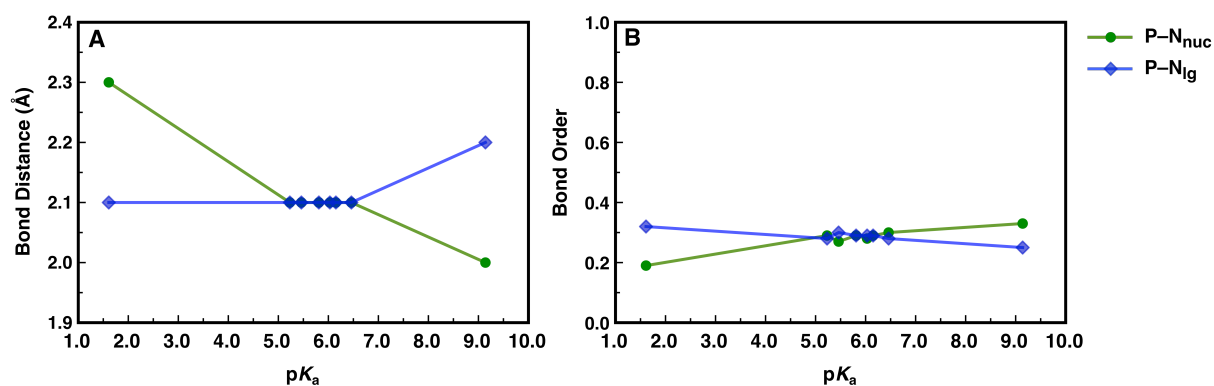


Figure 4: Two-dimensional reaction coordinate diagram showing the nature of the transition states calculated for the reaction of pyridine with pyridinio-N-phosphonates (red) studied here, as well as for the solvent-assisted phosphate monoester dianion hydrolysis and alkaline hydrolysis of sulfonate esters, fluorophosphates and aryl phosphate diesters (blue, orange, green and yellow respectively) obtained in our previous studies^{13,39-41}. The reaction coordinate is presented in terms of Wiberg bond indices⁴⁹ for the P(S)-nucleophile and P(S)-leaving group bonds respectively, calculated using natural bond orbital (NBO) analysis⁵⁰ at the ω B97X-D/6-31+G(d) level of theory, with the exception of fluorophosphates and phosphate diesters, where the bond indices were calculated at the B3LYP/6-31+G(d) level of theory for consistency with the original studies,^{39,40} as described in the **Methodology** section.

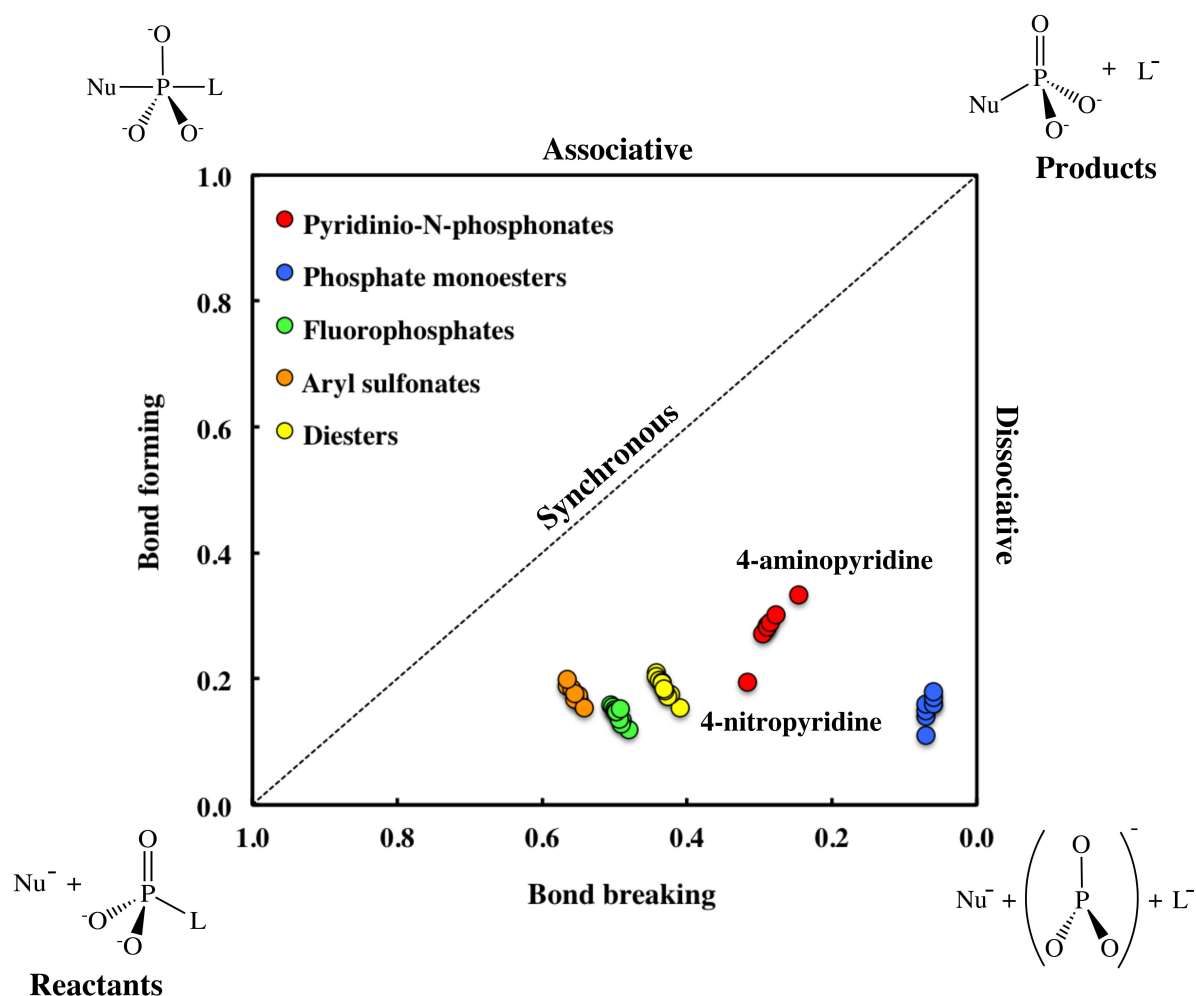


Figure 5: Atomic partial charges of nucleophile and leaving group pyridyl groups, and the central PO₃ group, calculated at the transition states for the reactions of substituted pyridinio-*N*-phosphonates with pyridine. All partial charges are calculated using the Merz-Kollman scheme^{51, 52} at the SMD- ω B97X-D/6-31G*// SMD- ω B97X-D/6-31+G* level of theory. For the corresponding raw data, see **Table 3**.

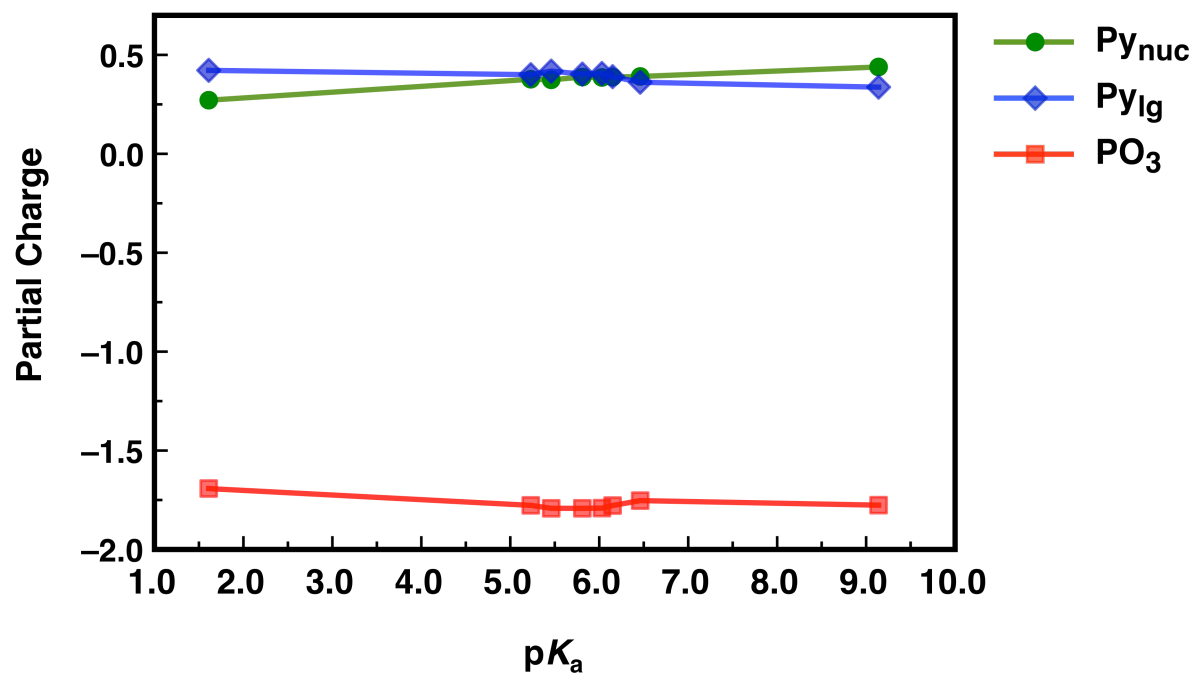


Table 1: Experimental and calculated rate constants and activation free energies for the reactions of substituted pyridinio-*N*-phosponates with pyridine.^a

	pK_a	k_{exp}	k_{calc}	$\log k_{\text{exp}}$	$\log k_{\text{calc}}$	$\Delta G^\ddagger_{\text{calc}}$
4-nitropyridine	1.61	--	1.1×10^4	--	4.059	9.5
pyridine	5.23	--	9.6		0.981	13.7
isoquinoline	5.46	1.43 ± 0.05	6.8	0.155	0.834	13.9
3-methylpyridine	5.81	0.81 ± 0.05	26.3	-0.092	1.420	13.1
3-aminopyridine	6.03	0.78 ± 0.05	4.9	-0.108	0.687	14.1
3,5-dimethylpyridine	6.15	0.34 ± 0.1	22.2	-0.469	1.347	13.2
3,4-dimethylpyridine	6.46	0.26 ± 0.05	0.76	-0.585	-0.119	15.2
4-aminopyridine	9.14	$6.24 \pm 1.310 \times 10^{-4}$	0.05	-3.205	-1.292	16.8

^a Shown here are the leaving group pK_a , the calculated and experimental rate constants ($\text{M}^{-1} \text{s}^{-1}$), the log of the rate constants, and the calculated activation free energies (kcal mol^{-1}). The calculated activation free energies were converted to the corresponding rate constants using transition state theory, and converted to second order rate constants by correcting for the entropic cost of bringing the reacting fragments into the reacting cage ($K=0.017 \text{ M}^{-1}$), following ref. ⁵⁵. The experimental values were obtained from ref. ¹⁷. pK_a values were obtained from ref. ⁶³ for 4-nitropyridine, ref. ⁶⁴ for pyridine, and ref. ¹⁷ for all other compounds.

Table 2: Calculated bond distances (Å) and bond orders to the incoming nucleophile (P-N_{nuc}) and departing leaving group (P-N_{lg}) at the transition states for the reactions of substituted pyridinio-*N*-phosphonates with pyridine.^a

	p <i>K</i> _a	Bond Distance		Bond Order	
		P-N _{nuc}	P-N _{lg}	P-N _{nuc}	P-N _{lg}
4-nitropyridine	1.61	2.30	2.05	0.19	0.32
pyridine	5.23	2.14	2.12	0.29	0.28
isoquinoline	5.46	2.15	2.11	0.27	0.30
3-methylpyridine	5.81	2.13	2.12	0.29	0.29
3-aminopyridine	6.03	2.13	2.13	0.28	0.29
3,5-dimethylpyridine	6.15	2.12	2.13	0.29	0.29
3,4-dimethylpyridine	6.46	2.10	2.15	0.30	0.28
4-aminopyridine	9.14	2.04	2.21	0.33	0.25

^a All distances were obtained for the transition states for the attack of pyridine on the pyridinio-*N*-phosphonates optimized at SMD- ω B97X-D/6-31+G(d) level of theory. Wiberg bond indices⁴⁹ were calculated using natural bond orbital (NBO) analysis⁵⁰ performed at the same level of theory. p*K*_a values were obtained from ref. ⁶³ for 4-nitropyridine, ref. ⁶⁴ for pyridine, and ref. ¹⁷ for all other compounds.

Table 3: Calculated partial charges on key reacting atoms at the transition states for the reactions of substituted pyridinio-*N*-phosphonates with pyridine.^a

	pK_a	Py_{nuc}	Py_{lg}	PO_3
4-nitropyridine	1.61	0.271	0.422	-1.692
pyridine	5.23	0.377	0.400	-1.777
isoquinoline	5.46	0.374	0.418	-1.792
3-methylpyridine	5.81	0.388	0.403	-1.792
3-aminopyridine	6.03	0.386	0.406	-1.791
3,5-dimethylpyridine	6.15	0.388	0.390	-1.778
3,4-dimethylpyridine	6.46	0.391	0.362	-1.753
4-aminopyridine	9.14	0.439	0.337	-1.776
<Partial Charge>	--	0.377±0.044	0.392±0.027	-1.769±0.031

^a Shown here are the leaving group pK_a s, as well as the partial charges on the nucleophile (Py_{nuc}) and leaving group nitrogen (Py_{lg}) pyridyl groups, and the central PO_3 group. pK_a values were obtained from ref. ⁶³ for 4-nitropyridine, ref. ⁶⁴ for pyridine, and ref. ¹⁷ for all other compounds. Shown here are also the average partial charges over all leaving groups, and the corresponding standard deviations. All partial charges are calculated using the Merz-Kollman scheme^{51,52} at the SMD- ω B97X-D/6-31G**/ SMD- ω B97X-D/6-31+G* level of theory. Note that the explicit water molecules were removed for the charge calculation, as described in the **Methodology** section.

Table of Contents Graphic

